Molecule-Driven Substrate Reconstruction in the Two-Dimensional Self-Organization of Fe-Phthalocyanines on Au(110)

7 AUTHORS, INCLUDING:

Sara Fortuna
University of Udine
15 PUBLICATIONS **151** CITATIONS

SEE PROFILE

Maria Grazia Betti
Sapienza University of Rome
159 PUBLICATIONS **1,961** CITATIONS

SEE PROFILE

Arrigo Calzolari
Italian National Research Council
108 PUBLICATIONS **1,893** CITATIONS

SEE PROFILE

Stefano Fabris
Italian National Research Council
75 PUBLICATIONS **5,988** CITATIONS

SEE PROFILE

Molecule-Driven Substrate Reconstruction in the Two-Dimensional Self-Organization of Fe-Phthalocyanines on Au(110)

Sara Fortuna,*[†,‡] Pierluigi Gargiani,[§] Maria Grazia Betti,[§] Carlo Mariani,[§,‖] Arrigo Calzolari,[⊥] Silvio Modesti,[#,¶] and Stefano Fabris[†,‡]

[†]CNR-IOM DEMOCRITOS, Theory@Elettra group, S.S. 14, km 163.5, I-34149 Trieste, Italy

[‡]SISSA, Via Bonomea 265, I-34136, Trieste, Italy

[§]Physics Department, Sapienza University of Rome, Piazzale A. Moro 5, I-00185 Roma, Italy

[‖]CNIS, CNISM, Sapienza University of Rome, I-00185 Roma, Italy

[⊥]CNR-NANO, Institute of Nanoscience, S3 Center, I-41125 Modena, Italy

[#]Physics Department, University of Trieste, via Valerio 2, I-34127 Trieste, Italy

[¶]CNR-IOM TASC, S.S. 14, km 163.5, I-34149 Trieste, Italy

ABSTRACT: The structural patterns formed by molecular self-assembly at surfaces are usually controlled by the relative strengths of the intermolecular and molecule−substrate interactions. An additional steering effect is present when the substrate can easily reconstruct upon molecular adsorption, which therefore drives a self-templating effect on the metal support. This is here demonstrated for the model case of Fe-phthalocyanine molecules adsorbed on the Au(110) surface. Scanning tunneling microscopy shows that molecular adsorption promotes a local (1 × 5) surface reconstruction, which drives the assembly of molecular chains along the $[1\bar{1}0]$ direction. The order and periodicity of the molecular assemblies are determined with low energy electron diffraction patterns. Density functional theory calculations reveal the energetic origins of the molecule-driven substrate reconstruction. Since the function of molecular overlayers at surfaces is strongly correlated to their structure, these results have implications in the design of new metal/molecular interfaces.
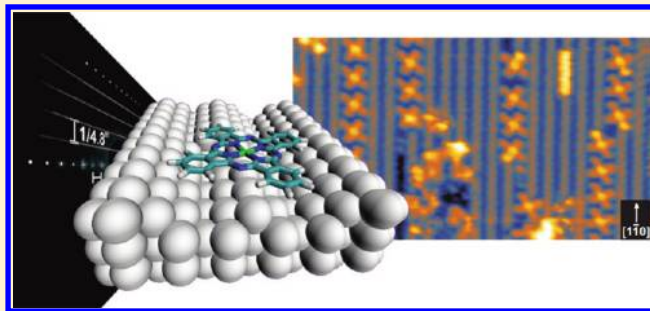
I. INTRODUCTION

Self-organized metallorganic molecules adsorbed on surfaces can form ordered patterns exposing regular arrays of coordinated metallic ions.[1,2] These have several potential applications in both the energy[3,4] and high-tech sectors[5,6] since coordinated metals adsorb visible light, catalyze chemical reactions, and can act as single-atom magnets.[7,8] These characteristics make them ideal candidates for catalytic[9,10] and data-storage devices,[11,12] whose functioning depends on both the structural and electronic properties of the self-assembly and is determined by the nature of the coordinated metal, the organic ligands, and the underlying surface. In this context, an understanding of the molecule substrate interplay is a key aspect in the design of new molecular-based devices.[13,14]

Metal-supported metal-phthalocyanines (MPc, Figure 1a) are an ideal case system for the study of the molecule/substrate interplay. Phthalocyanines are large conjugated cross-shaped molecules able to coordinate most of the transition metals and self-assemble on surfaces into a variety of structures presenting isolated islands,[15] chains,[16−18] disordered,[19] square,[20] hexagonal,[21] and Kagome[22] patterns. Combined density functional theory (DFT) and scanning tunneling microscopy (STM) studies have shown how the structures depend on the interplay among

(i) the coverage and temperature, (ii) the metal−surface interaction, and (iii) the nature of the surface. At low coverage, the molecular arrangement is mostly controlled by the metal−surface interaction. When there is no metal−surface interaction, such as in the case of metal-free H_2Pc adsorbed on the flat Ag(111), the intermolecular interactions drive the formation of ordered islands.[15] Similar ordered structures are observed for FePc and MnPc on Pb(111), while these molecules adsorb as isolated on Au(111) due to the stronger substrate−metal interaction.[23] At higher coverages, the FePc molecules form ordered compact patterns on Au(111).[20] The range of the ordering of the high-density patterns also depends on the metal−surface interaction strength. This is shown by the SnPc, CoPc, and PbPc series, which display an increasing interaction strength with Ag(111):[19] SnPc forms long-range ordered monolayers, CoPc shows only local order, and PbPc is disordered. Therefore, on flat metal surfaces, when the intermolecular interactions are stronger than metal/surface ones, MPc's assemble into ordered aggregates. However, the details of that order depend on the symmetry and
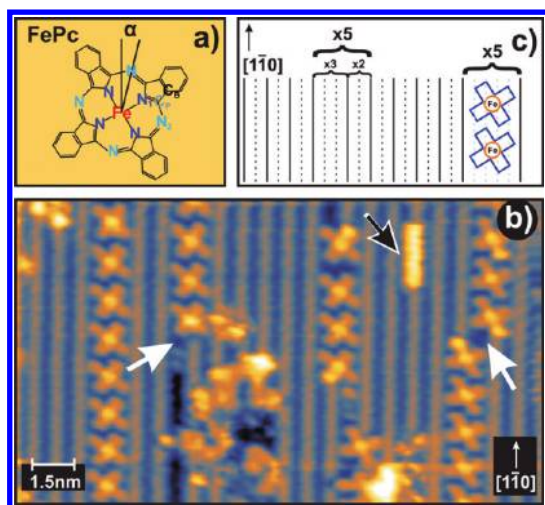
Figure 1. Self-assembly of FePc molecular chains. (a) Structure of the FePc molecule. (b) STM topography collected at −0.77 V and 0.4 nA in constant current mode at $T = 60$ K on a FePc/Au(110) at a coverage of about 0.1 SL of FePc; the black arrow indicates an added row of Au atoms, and the white arrows indicate a sequence of ×2 ×3 Au reconstructions. (c) Scheme of the surface reconstruction induced by molecular adsorption. The continuous lines refer to Au atomic rows and the dotted lines to the Au missing rows.

periodicity of the substrate: square and hexagonal lattices have been observed on (111) surfaces,[19,20,24] while Kagome lattices are observed on graphene.[22]

Highly anisotropic surfaces can act as templates for the self-assembly, as in the case of (110) surfaces of fcc metals, where organic molecules have been observed to align along the $[1\bar{1}0]$ direction.[16−18,25−32] Here however also the propensity of the surface toward reconstruction comes into play, i.e., its tendency to assume a different structure compared to that of the truncated bulk. A special case is that of the Au(110) surface, which is known to easily reconstruct. Indeed the metal−surface interaction between aromatic molecules and Au(110) induces the rearrangement of the naturally reconstructed 1 × 2-Au(110) surface into a 1 × 3 structure.[27,29,33] For the CuPc system also ×5 reconstructions have been proposed.[17] Here we will study another instance of molecule-driven surface reconstruction, namely, the FePc on Au(110). This interplay between the metall-organic molecule and a plastic substrate will be systematically studied in terms of STM, low-energy electron diffraction (LEED), and DFT calculations.

II. METHODS

A. Experimental Section. Experiments have been performed in an ultrahigh-vacuum (UHV) system equipped with an STM platform and ancillary equipment for sample preparation and cleaning. The clean Au(110)-1 × 2 surface was obtained by sputter-annealing cycles (1000 eV, 720 K), and surface cleanness and order were checked with STM and LEED, respectively. The STM topographic images have been obtained by a homemade UHV scanning tunneling microscope operating between 5 and 300 K in the constant tunneling current mode using a gold tip. FePc was sublimated from a resistively heated quartz crucible in UHV, and the nominal thickness was measured via oscillating quartz microbalances. FePc has been deposited on the clean Au(110) substrate kept at about 100 °C, with a constant deposition rate of about 0.5 Å/min, from low coverage to about a

compact single layer (SL) of aligned molecules. The samples were then cooled slowly to 60 K.

B. Theory. The DFT calculations were performed with the Perdew−Burke−Ernzerhof generalized gradient corrected approximation (PBE-GGA) for the exchange and correlation energy functional.[34] The spin-polarized Kohn−Sham equations were solved in the plane-wave pseudopotential framework, as implemented in the PWscf code of the QUANTUM ESPRESSO distribution.[35,36] The valence wave functions were described by a plane-wave basis limited to 30 Ry, while the charge density Fourier representation was limited by a cutoff of 300 Ry. The simulation of the gas-phase molecules, clean surfaces, and combined FePc/Au(110) systems were studied with $(\vec{r} \times \vec{d} \times \vec{h})$ orthorhombic supercells.

The isolated gas-phase molecule was simulated with $r = d = 42.34$ Å and $h = 21.17$ Å. The interaction energy within unsupported molecular chains was calculated by using a cell with $r = 20.90$ Å and $h = 16.51$ Å and by varying the intermolecular distance d and the orientational angle α (Figure 1a).

We considered a set of clean Au(110) surfaces, namely, the 1 × 1, 1 × 2, and all the possible 1 × 3 and 1 × 5 reconstructions. Each surface, modeled by five atomic layers, was relaxed by keeping the two bottom layers fixed at the bulk positions. The surface energy E_{surf} was calculated on thicker supercells ranging from 11 to 15 atomic layers. The surface energies were calculated using a regular grid of **k**-points comparable to 18−25−1 on the 1 × 1 surface, together with an interlayer distance of 10 Å. Our results are in line with the available literature.[37]

The combined FePc/Au(110) system was modeled by adsorbing the FePc molecule on all the possible ×5 reconstructions of the Au(110) surface. These systems were described with periodic supercells having lateral extension corresponding to (5 × 5) primitive unit cells of the Au(110) surface. The latter was modeled with a slab consisting of five atomic layers, separated in the z direction by more than 13 Å of vacuum, with the lattice parameter set to the calculated equilibrium one (4.18 Å). During the structural relaxations, the lowermost two layers were kept fixed at their bulk-like coordinates. Integrals in the Brillouin zone were performed on the Γ-point together with a Marzari−Vanderbilt smearing of 0.02 Ry. STM images were simulated within the Tesoff−Hamann approximation at different applied bias.[38]

III. RESULTS

A. Structure of Self-Assembled Molecular Chains: STM. The STM image of the molecular self-assembly resulting from depositing ∼0.1 SL of FePc molecules on the Au(110) surface is displayed in Figure 1b. The cross-like shape of the unsupported molecule (Figure 1a) is preserved upon adsorption on the surface and can be clearly seen in the STM image, together with a bright central spot in correspondence to the Fe molecular center. The majority of the molecules assembles into chains aligned along the $[1\bar{1}0]$ direction. These chains span ×5-reconstructed surface channels (see Figure 1c), hence showing that molecular adsorption and self-assembly promote the local formation of a 5-fold reconstruction of the Au(110) surface along [001], molding a templated substrate. Besides the ×2 reconstruction of the pristine Au(110) surface (8.16 ± 0.08 Å wide), the presence of 12.34 ± 0.08 Å wide channels points to a ×3 reconstruction. The ×3 defects are necessary to accommodate the ×5 reconstruction induced by the FePc self-assembly (see below). Moreover, the molecular chains terminate preferentially at these ×3 surface defects (see white arrows in Figure 1b), which
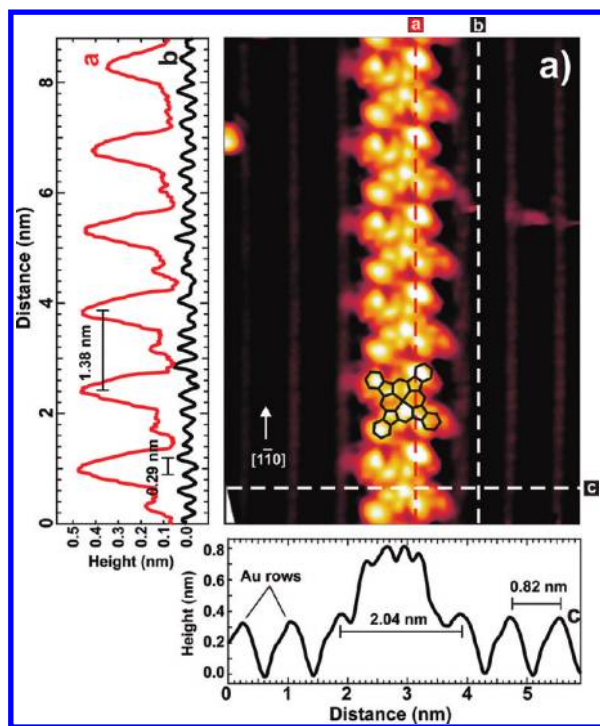
Figure 2. STM topography image of a single molecular row, $V = -1.000$ V, $I = 0.2$ nA at $T = 4$ K. The height profiles reported in the left (traces a and b) and bottom (trace c) panels are relative to the dotted lines drawn on the STM image panel.

Figure 3. Experimental (left panels) and theoretically simulated (right panels) STM images of FePc on Au(110), taken at different bias: −0.170 V (upper images) and −1.000 V (lower images). Simulated images correspond to the lowest-energy configuration discussed later in the text.

are common on the clean Au(110) surface at high temperature[39] or in the presence of adsorbates.[40−43] At variance, isolated FePc molecules tend to adsorb at step edges (not shown).

Each FePc molecule in the self-assembled chains is rotated by an average angle $\alpha = 13 \pm 2°$ with respect to the $[1\bar{1}0]$ direction (Figure 1a). We identify the emergence of two chain arrangements differing in the rotational angle of the FePc molecules, $\pm\alpha$. A slight asymmetry between the two orientational angles in Figure 1b can be attributed to the sample drift during acquisition.

Figure 2 displays a high-resolution STM image of an isolated FePc chain (central panel) together with the height profiles sampling of the molecular chains and the clean Au surface along $[1\bar{1}0]$ (a,b, left panel), as well as along $[001]$ (c, bottom panel). These data support a flat-lying adsorption geometry of the FePc molecules in the chains within an accuracy of 5°, and this is consistent with previous studies of metal Pc (e.g., Fe, Co) adsorbed on the Au(110) surface.[44] The areas of Au(110) surface neighboring the chains are not affected by the molecular adsorption since they are identical to the clean Au(110) 1 × 2 surface (Figure 2, trace c and trace b).[43,46]

High-resolution STM images taken at two different bias voltages (−1.000 and −0.170 V, both sampling occupied states), along with the theoretically simulated STM images computed at the same bias conditions, are shown in Figure 3. The low-bias STM (top panel) shows a brighter intensity of the Fe center than the benzene lobes, while the higher-bias image (bottom panel) shows brighter pyrrole and benzene structures. This behavior is confirmed by the theoretical STM simulations (Figure 3, right panels), which reproduce the same bright spot contrast between the central Fe ion and the aromatic macrocycle as displayed in the experiments.
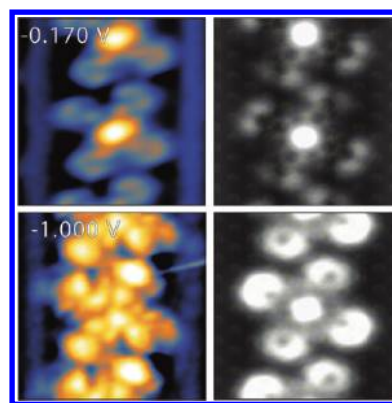
This apparent height variation is consistent with an actual distribution in density of occupied states at different binding energies (BEs) with respect to the Fermi level. In fact, the molecular interaction with the underlying substrate mediated by the molecular orbitals localized on the Fe ion gives rise to a low-BE structure, which is responsible for the central bright spot at low bias.[30,45] On the other hand, molecular states lying at higher BE[30] are localized on the aromatic rings and generate the STM image distributed on the four molecular lobes appearing at higher bias. In this latter case, a slight asymmetry between the two perpendicular arms of the single molecules is visible and is accounted for by the theoretical simulated image, due to a broken symmetry upon adsorption on Au(110) resulting in an upturn of two opposite phthalocyanine lobes that will be commented on later.

The STM atomic resolution of the Au atoms along the $[1\bar{1}0]$ direction allows for a precise determination of the periodicity of the FePc molecules within the chains. The molecules are spaced along $[1\bar{1}0]$ by 1.38 ± 0.02 nm, corresponding to 4.78 ± 0.05 lattice units of the Au(110) surface. Note that the periodicity of the molecular chain is incommensurate with the metal support. This suggests the lack of a preferential absorption site along the Au channels, which is confirmed by the calculations described in the following.

B. Interchain Long-Range Ordering. At higher coverages, the molecular chains described above assemble into a secondary superstructure leading to a compact molecular overlayer. Figure 4 displays a STM image of one compact domain resulting from depositing 0.7 SL of FePc on Au(110). The structure observed for isolated chains is maintained, with the FePc chains stacked along the $[001]$ direction and separated by one row of Au atoms.

The intrachain molecular arrangement seems not to be much influenced by the interchain interaction. In particular, the molecule-to-molecule distance within the chain (d) and the molecular angular orientation with respect to the chain direction (α) are the same as those observed in the isolated chains (Figure 2), 1.38 nm and 13°, respectively. Similarly to what is observed for the isolated chain, the periodicity along $[1\bar{1}0]$ of the FePc molecules in the compact domains is incommensurate with the underlying surface lattice. The assembly along the $[001]$ direction is commensurate with the Au(110) ×5 reconstructed periodicity. This STM image shows three chains aligned and a fourth chain shifted. The lack of a specific adsorption site for the
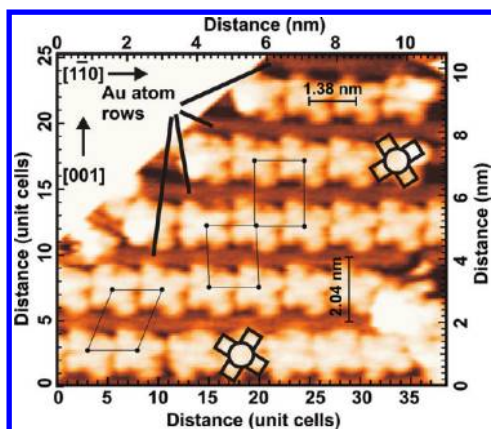
Figure 4. STM image collected on a ×5 ordered zone in constant current mode ($V = -1.2$ V, $I = 0.1$ nA). The FePc molecules assume two specular orientations with respect to the Au channel direction as schematized by the molecule sketches.
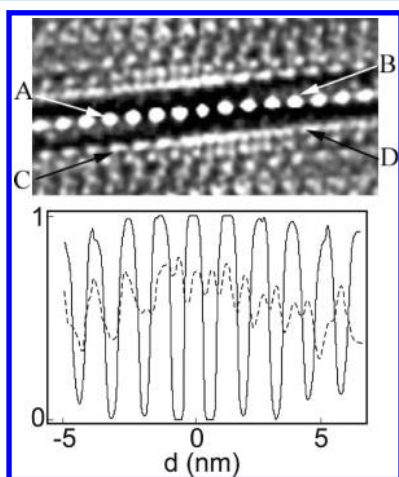
Figure 5. Top panel: self-correlation map of the positions of the center of the FePc molecules obtained from a STM image containing 250 molecules at about 40% of the saturation coverage. Bottom panel: line profiles of the self-correlation along the $[1\bar{1}0]$ oriented lines from A to B (solid line) and from C to D (dashed line); the first profile shows the correlation between the positions of the molecules in the same chain and the second profile the correlation between the position of a molecule in one chain and the positions of the molecules in the adjacent chain.

FePc in the Au channels allows the chains to shift along the $[1\bar{1}0]$ direction. A statistical analysis of the alignment among chains performed on several images shows an interchain correlation spanning only a few nanometers. To evaluate the long-range ordering and the coherence domain of the FePc chains from local-scale topography, we show in Figure 5 the self-correlation calculation of a STM image displaying several hundreds of molecules. The self-correlation between the positions of hundreds of molecules (see Figure 5) shows a well-defined modulation along the $[1\bar{1}0]$ direction corresponding to the nearly uniform spacing between molecules in the same row (AB segment and solid line in the bottom panel) and also an appreciable modulation along the CD segment (dashed line). This weaker modulation indicates that the shift of the position of the molecules in a row with respect to that of the nearest row is not completely random. The STM images show that there is short-range order between the
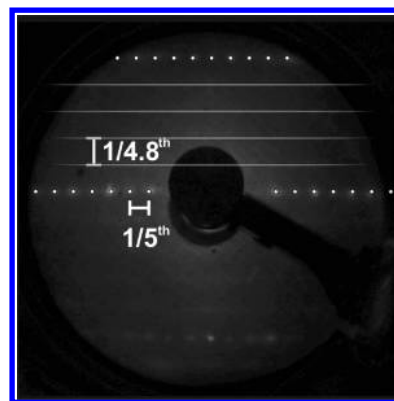
Figure 6. LEED image relative to the FePc ×5 single layer with a superposition of the expected pattern obtained from STM and a theoretical surface model. The ×5 spots in the $[001]$ direction indicate the long-range ordering of the molecular chains along this direction. The stripes stacked along the perpendicular $[1\bar{1}0]$ direction are due to the absence of a definite phase among the adjacent molecular rows.

position of the molecules in adjacent chains in regions a few nanometers wide.

To verify the long-range order of the one-dimensional (1D) FePc chains aligned along the Au(110) channels, we report a LEED image of the ×5 single layer in Figure 6. The diffraction pattern is characterized by well-defined spots along the $[001]$ direction of the integer-order diffraction lines, as the result of the ×5 commensurate Au reconstruction, and less intense stripes stacked along the $[1\bar{1}0]$ direction, corresponding to noninteger diffraction orders. An accurate analysis of the diffraction pattern on several LEED images (not shown here) leads to a periodicity of 4.79 ± 0.03 along the $[1\bar{1}0]$ direction, corresponding to 1.38 nm intrachain spacing (almost ×5 periodicity), which is indeed in very good agreement with both the STM and DFT results (see below).

C. Energetics of FePc Self-Assembly and Au(110) Reconstruction: DFT Calculations. DFT calculations are used to provide insights into the energetics governing the molecular self-assembly and the observed substrate reconstruction. To do so, we first decouple the molecular chains from the substrate and address (i) the maximum packing density in the unsupported molecular chains and (ii) the surface energy of the clean Au(110) surface reconstructions. Then we focus on the molecule-induced reconstruction of Au(110) by simulating the complete FePc/Au(110) system.

1. Intrachain Molecular Periodicity. The lowest-energy linear assembly of coplanar unsupported FePc molecules is determined by calculating their interaction energy (eV/molecule, Figure 7a) as a function of their intermolecular distance (d) and rotational angle with respect to the chain axis (α). This analysis predicts that the maximum molecular density along the linear chain corresponds to $d_0 = 1.42 \pm 0.03$ nm and $\alpha_0 = 18° \pm 1°$. In this optimal configuration (Figure 7b), the molecules are interdigitated, and the corresponding structural parameters are in agreement with the experimental values measured on the surface-supported FePc chains ($d = 1.38 \pm 0.02$ nm and $\alpha = 13° \pm 2°$). This quantitative agreement shows that the measured periodicity and relative rotation of the molecules along the $[1\bar{1}0]$ surface channels of the reconstructed surface stem from steric effects. In addition, the equilibrium intermolecular distance is incommensurate with the surface periodicity along
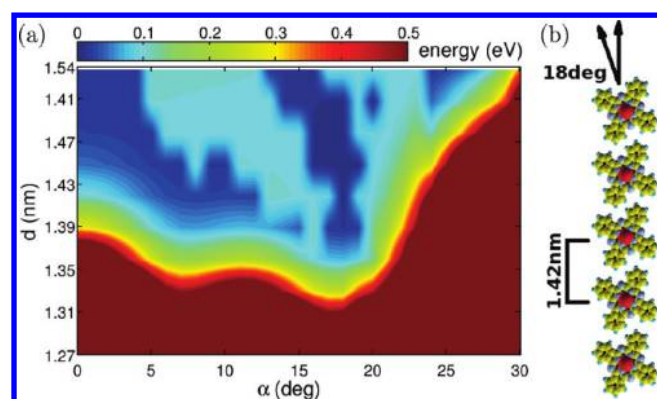
Figure 7. FePc energy landscape. (a) FePc energy as a function of its orientational angle α and the Fe–Fe distance d along the $[1\bar{1}0]$ direction, with zero-point energy corresponding to the minimum energy configuration. (b) Minimum energy configuration, with $d = 1.42 \pm 0.03$ nm and $\alpha = 18 \pm 1°$.

Figure 8. Surface energy $\Delta\gamma$. The zero of the scale corresponds to the surface energy $\gamma_{\times 2}$ of the 1×2-Au(110) naturally reconstructed surface (bottom left). The lowest-energy $\times 5$ surface is the $\times 5$**A** (bottom right) which corresponds to the $\times 2$ $\times 3$ observed in STM images (as in Figure 1).

$[1\bar{1}0]$ ($d_0 = 4.8$ Au(110) lattice units), similarly to what is observed for the surface-supported molecular chains. This indicates the absence of a preferential adsorption site along the reconstructed $[1\bar{1}0]$ surface channels, which will be further validated in the following sections.

The calculated energy surface shows that isolated molecules can align and reach the equilibrium configuration with roto-translations without incurring any energy barrier. Note that the energy landscape surrounding the global minimum is relatively shallow. The intermolecular distance can decrease up to 1.37 nm with an energy cost of just 0.1 eV/molecule. At closer distances, the intermolecular repulsion comes into effect and yields a steep potential.

2. Au(110) Surface Reconstructions. The plasticity of the Au(110) surface with respect to its reconstructions is studied by comparing the surface energy γ of a set of surfaces with periodicities relevant to the experiments reported above. Previous theoretical works already addressed some of these reconstructions, for instance, the $\times 1$, $\times 2$, and one of the three possible $\times 3$ reconstructions.[40,47−51,53] Here we have included the full set of the $\times 3$ and the $\times 5$ surfaces displayed in Figure 8. In agreement with the literature, the $\times 2$ reconstruction is predicted to have the lowest surface energy, $\gamma_{\times 2} = 49.4$ meV/Å². This value is taken as a reference for the surface energetics described by: $\Delta\gamma = \gamma - \gamma_{\times 2}$ (Figure 8). The upper boundary is the energy of the unreconstructed $\times 1$ surface, $\Delta\gamma_{\times 1} = 4.3$ meV/Å².

All $\times 3$ reconstructions have comparable surface energies (within ~2 meV/Å²), with the $\times 3$**A** being the lowest one with $\Delta\gamma_{\times 3A} \sim 0.2$ meV/Å². Instead, the $\times 5$ reconstructions span a much larger energy window (1−3 meV/Å²), most of them having surface energies lower than $\Delta\gamma_{\times 3A}$. In particular, this analysis identifies two surface structures ($\times 5$**A** and $\times 5$**B**) whose surface energy is close to $\gamma_{\times 2}$. In particular, the lowest-energy one, $\times 5$**A**, results from alternating side-by-side the $\times 2$ and $\times 3$**B** surfaces and is compatible with the $\times 5$ Au(110) reconstructions visible in the STM images at the terminations of the FePc chains (Figure 1). The small energy differences between the $\times 2$ and some $\times 5$ reconstructions confirm the plasticity of Au(110), which can easily undergo local reconstructions by forming surface line defects. Note that these energy differences, apparently very small, when referred to the area of the unit cell used to calculate them (see E_{rec} in Table 1) clearly differentiate among the possible reconstructions on the basis of the calculated accuracy.
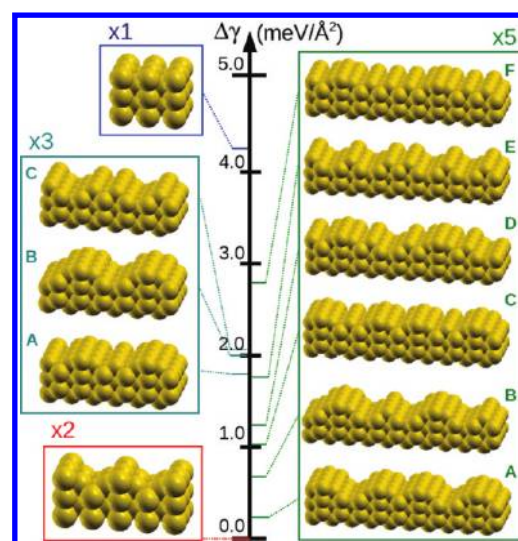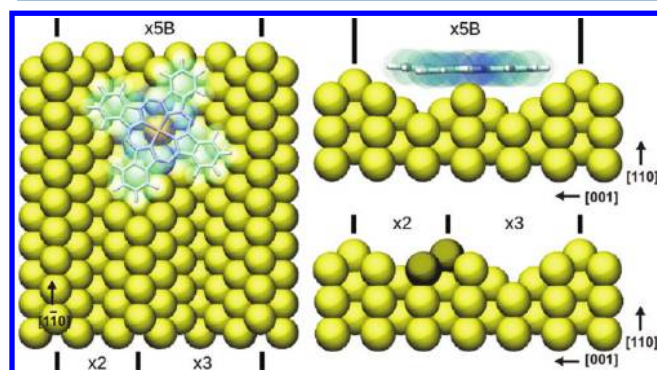
3. Molecule-Induced Surface Reconstruction. Here we address the combined system consisting of a molecular FePc chain supported by different reconstructions of the Au(110) surface. This allows us to predict the surface structure underneath the molecular chains as well as to identify the origins of this molecule-induced surface reconstruction. First we look at the corrugation of the adsorption energy as a function of the binding site along $[1\bar{1}0]$. The energy difference between the FePc on top and bridge sites is below 0.08 eV, showing the absence of a preferential adsorption site in agreement with the noncommensurate periodicity along $[1\bar{1}0]$ observed experimentally. Hence the molecules can freely translate in the channels to maximize the chain density with little constraint from the lattice periodicity.

In the following, we discuss the energetics obtained for the most favorable top adsorption site of the three lowest-energy $\times 5$ reconstructions ($\times 5$**A−C**). For comparison, we also consider the molecule adsorbed on the highest-energy flat surfaces $\times 5$**F** and $\times 1$. We propose that the molecule−substrate energetics is governed by two contributions: (i) the energy of molecular adsorption on a given surface reconstruction, $E_{ads} = E_{tot} - E_{FePc}^{\infty} - E_{surf}^{\infty}$, and (ii) the energy cost necessary to form that surface, $E_{rec} = \Delta\gamma \cdot A$. In these definitions, E_{tot} is the total energy of the relaxed FePc/Au(110) system; E_{FePc}^{∞} is the energy of an isolated FePc; E_{surf}^{∞} is the energy of the isolated surface; and A is the area of the surface. The lowest-energy configuration for the molecule/Au(110) interface is the one with the most negative $\Delta E = E_{ads} + E_{rec}$. We report this energetic analysis in Table 1. We wish to remark that we here compare the internal energy and not the system free energy. At finite temperature, the contribution of vibrational entropy to the free energy is always present and can be estimated on the basis of the vibrational frequencies of the system. However, for the case of Au, the contribution of the vibrational entropy is very small, about 1.8% of the internal energy at room temperature for bulk, and increases to 2.2% in the case of a small cluster exposing almost exclusively surface atoms.[52] As the STM images were collected by annealing the system below 60 K, we expect this contribution to be negligible.

Table 1. Calculated FePc Adsorption (E_{ads}) and Substrate Reconstruction (E_{rec}) Energies for Different ×5 Au(110) Surfaces[a]

	×5B	×5A	×5C	×5F	×1
ΔE (eV/cell)	−0.52	−0.35	−0.16	0.18	0.55
E_{ads} (eV/cell)	−0.73	−0.42	−0.48	−0.69	−0.77
E_{rec} (eV/cell)	0.21	0.07	0.31	0.86	1.32

[a]Structures are ordered (left to right) as a function of the energy gain $\Delta E = E_{ads} + E_{rec}$.

Figure 9. Model of molecular adsorption and surface reconstruction resulting from the calculated energetics for the FePc/Au(110) system. The top and side views are reported in the left and right panels, respectively. The ×5B reconstruction underneath the molecule is obtained by removal of the darker Au atoms from the ×5A surface.

It turns out that E_{ads}, which takes into account contributions from the surface and the molecular deformations, the intermolecular interactions, and the molecule−surface interaction, is the largest for the surfaces displaying a mirror symmetry along $[1\bar{1}0]$ with respect to the adsorption site (×5B, ×5F, and ×1, see Table 1). This leads to symmetric adsorption geometries that allow for a direct and shorter Fe−Au bond and reduce the molecular distortions. The reconstruction energy is instead minimum for the ×5A surface, which does not have a $[1\bar{1}0]$ mirror symmetry with respect to the FePc adsorption site; in this latter case the molecule is adsorbed in a highly asymmetric position, leading to a distorted geometry. Overall, although the E_{ads} is exothermic for all these surfaces, the energy balance $E_{ads} + E_{rec}$ predicts the presence of the ×5B reconstruction underneath the adsorbed FePc chains. This configuration is also the one with the shortest Fe−Au distance, 2.74 Å (to be compared with 3.87 Å for ×5A). Quite interestingly, the adsorption on the flat ×5F or ×1 surfaces is ruled out by energetic arguments: even if E_{ads} is negative for both these flat surfaces, their large surface reconstruction energies (E_{rec} = 0.86−1.32 eV/cell) lead to a positive ΔE in both cases.

These simulations suggest a model of adsorption and surface reconstruction, as that reported in Figure 9. The experimental STM images show that the FePc molecules assemble along $[1\bar{1}0]$ and induce a ×5 reconstruction of the Au(110) surface along $[001]$. Our simulation predicts that the clean ×5 reconstructed surface is the ×5A of Figure 8, obtained by an alternating sequence of ×2 ×3 reconstructions. The resulting ×5 channels are compatible with the molecular size, and the FePc molecules adsorb and self-organize into these ×5 reconstructed channels. The shallow corrugation of the adsorption energy along the channels allows for maximizing the chain density by forming an incommensurate molecule/metal interface, whose periodicity is determined by molecular steric

effects. The agreement of these predictions with the experimental observations allows us to draw considerations on the nonvisible portion of the system. Underneath the molecules, the energetics predict the formation of a symmetric ×5B reconstruction, which maximizes E_{ads}. The surface ×5B formally differs by the ×5A by removal of two Au rows (indicated by a darker color in the right panel of Figure 9). Actually, a small chain of Au atoms removed by the molecules and rearranged on top of clean Au areas is clearly visible in Figure 1, thus confirming this theoretical analysis. In this configuration, three effects are observed. On a larger scale, the molecule induces a symmetric reconstruction of the surface within the ×5 channels, allowing for the Fe center to adsorb directly on a Au row. The rotation of the molecules brings two of the phenylene rings closer to the lateral Au rows than the other two. As a result, the former groups are forced to bend upward, breaking the 4-fold molecular symmetry and leading to the slight asymmetry observed in the STM images (Figure 3). Finally, the FePc molecule induces a smaller scale effect on the underlying surface, as the Au atoms move away from the benzene lobes following the molecular profile. At the molecular chain terminations, the ×5 periodicity can be maintained at little energy cost, but the surface is predicted to reconstruct back into a ×5A structure, which is the lowest energy ×5 clean Au(110) surface (Figure 9).

IV. CONCLUSIONS

In this paper, we studied the molecule-driven surface reconstruction of the FePc on Au(110) as a case study to understand whether and up to which extent the molecule−substrate interplay can induce a self-templating effect of the metal surface that can guide the linear self-assembly of a planar molecular system. By STM imaging, we observe ×5 reconstructions of the clean Au(110)-1 × 2 surface in correspondence to FePc molecular chains. At high coverage, we observe a regular patterning of the surface with FePc chains aligned along the reconstructed channels with each chain separated by a row of Au atoms. The diffraction patterns confirm the 1D ordering along the channels and a ×5 periodicity along the $[001]$ direction. DFT calculations predict that the periodicity along the 1D assembly is driven by intermolecular interactions. The calculated energetics show that the ×5 reconstruction formed by alternating ×2 ×3 ones (×5A) is expected to be a common surface defect due to its surface energy comparable to that of the naturally occurring ×2 reconstruction. Adsorption of a FePc molecule on these ×2 ×3 line defects yields a significant binding energy, although the calculated energetics predicts that a larger molecular binding is achieved by first reorganizing the metal surface underneath the molecule in a symmetric structure. The energy cost to reconstruct the surfaces into a more suitable template is largely compensated by the larger adsorption energy on this optimized substrate.

We have shown the delicate molecule/substrate interplay that leads to a molecule-induced reorganization of the substrate, enhancing its templating effect. While small rearrangement of the interface atoms has been often observed due to molecular adsorbates, as with FePc and perylene inducing different reconstruction patterns on the Au(111) surface,[54] larger reorganizations have seldom been reported: both CuPc[33] and pentacene[29,55] have been observed to drive the ×3 reconstruction of the Au(110) surface, and the ×5 reconstruction has been observed only in the case of CuPc[17] and FePc, in the current work. As the electronic properties of supported organic overlayers strongly depend on the structural properties of the interface, the study of molecular-driven surface reconstruction is a key aspect to take into account for the band gap engineering of novel devices.

■ AUTHOR INFORMATION

Corresponding Author

*Phone: +39 0 40 3787 317. Fax: +39 0 40 3787 528. E-mail: fortuna@sissa.it.

Notes

The authors declare no competing financial interest.

■ ACKNOWLEDGMENTS

■ REFERENCES

(1) Das, M. C.; Xiang, S.; Zhang, Z.; Chen, B. *Angew. Chem.* **2011**, *50* (45), 10510−10520.
(2) Barth, J. V.; Costantini, G.; Kern, K. *Nature* **2005**, *437*, 671−679.
(3) Imahori, H.; Umeyama, T.; Ito, S. *Acc. Chem. Res.* **2009**, *42* (11, Sp. Iss. SI), 1809−1818.
(4) Rusu, M.; Strotmann, J.; Vogel, M.; Lux-Steiner, M. C.; Fostiropoulos, K. *Appl. Phys. Lett.* **2007**, *90* (15), 153511.
(5) Kurmaev, E.; Shamin, S.; Galakhov, V.; Moewes, A.; Otsuka, T.; Koizume, S.; Endo, K.; Katz, H.; Bach, M.; Neumann, M.; Ederer, D.; Iwami, M. *Phys. Rev. B* **2001**, *64* (4), 045211.
(6) Papageorgiou, N.; Salomon, E.; Angot, T.; Layet, J.-M.; Giovanelli, L.; Le Lay, G. *Prog. Surf. Sci.* **2004**, *77* (5−8), 139−170.
(7) Gispert, J. R. *Coordination Chemistry*; Wiley-VCH Verlag GmbH & Co. KGaA: Weinheim, 2008.
(8) Swiegers, G.; Malefetse, T. *Chem. Rev.* **2000**, *100* (9), 3483−3537.
(9) Holliday, B.; Mirkin, C. *Angew. Chem.* **2001**, *40* (11), 2022−2043.
(10) Coperet, C.; Chabanas, M.; Saint-Arroman, R.; Basset, J. *Angew. Chem.* **2003**, *42* (2), 156−181.
(11) Gan, F. *Chin. Sci. Bull.* **2000**, *45* (6), 572−576.
(12) Terris, B.; Thomson, T. *J. Phys. D* **2005**, *38* (12), R199−R222.
(13) Service, R. *Science* **2002**, *295* (5564), 2398−2399.
(14) Ariga, K.; Hill, J. P.; Lee, M. V.; Vinu, A.; Charvet, R.; Acharya, S. *Sci. Technol. Adv. Mater.* **2008**, *9* (1), 014109.
(15) Kera, S.; Casu, M.; Bauchspieß, K.; Batchelor, D.; Schmidt, T.; Umbach, E. *Surf. Sci.* **2006**, *600* (5), 1077−1084.

(16) Papageorgiou, N.; Ferro, Y.; Layet, J.; Giovanelli, L.; Mayne, A.; Dujardin, G.; Oughaddou, H.; Le Lay, G. *Appl. Phys. Lett.* **2003**, *82* (15), 2518−2520.
(17) Floreano, L.; Cossaro, A.; Gotter, R.; Verdini, A.; Bavdek, G.; Evangelista, F.; Ruocco, A.; Morgante, A.; Cvetko, D. *J. Phys. Chem. C* **2008**, *112* (29), 10794−10802.
(18) Evangelista, F.; Ruocco, A.; Gotter, R.; Cossaro, A.; Floreano, L.; Morgante, A.; Crispoldi, F.; Betti, M. G.; Mariani, C. *J. Chem. Phys.* **2009**, *131* (17), 174710.
(19) Baran, J. D.; Larsson, J. A.; Woolley, R. A. J.; Cong, Y.; Moriarty, P. J.; Cafolla, A. A.; Schulte, K.; Dhanak, V. R. *Phys. Rev. B* **2010**, *81* (7), 075413.
(20) Cheng, Z. H.; Gao, L.; Deng, Z. T.; Jiang, N.; Liu, Q.; Shi, D. X.; Du, S. X.; Guo, H. M.; Gao, H.-J. *J. Phys. Chem. C* **2007**, *111* (26), 9240−9244.
(21) Casarin, M.; Di Marino, M.; Forrer, D.; Sambi, M.; Sedona, F.; Tondello, E.; Vittadini, A.; Barone, V.; Pavone, M. *J. Phys. Chem. C* **2010**, *114* (5), 2144−2153.
(22) Mao, J.; Zhang, H.; Jiang, Y.; Pan, Y.; Gao, M.; Xiao, W.; Gao, H. J. *J. Am. Chem. Soc.* **2009**, *131* (40), 14136.
(23) Jiang, Y. H.; Xiao, W. D.; Liu, L. W.; Zhang, L. Z.; Lian, J. C.; Yang, K.; Du, S. X.; Gao, H.-J. *J. Phys. Chem. C* **2011**, *115* (44), 21750−21754.
(24) Bobaru, S. C.; Salomon, E.; Layet, J.-M.; Angot, T. *J. Phys. Chem. C* **2011**, *115* (13), 5875−5879.
(25) Evangelista, F.; Ruocco, A.; Corradini, V.; Donzello, M. P.; Mariani, C.; Betti, M. G. *Surf. Sci.* **2003**, *531*, 123−130.
(26) Evangelista, F.; Ruocco, A.; Pasca, D.; Baldacchini, C.; Betti, M. G.; Corradini, V.; Mariani, C. *Surf. Sci.* **2004**, *566−568*, 79−83.
(27) Prato, S.; Floreano, L.; Cvetko, D.; De Renzi, V.; Morgante, A.; Modesti, S. *J. Phys. Chem. B* **1999**, *103*, 7788.
(28) Temirov, R.; Soubatch, S.; Luican, A.; Tautz, F. S. *Nature* **2006**, *444*, 350−353.
(29) Baldacchini, C.; Mariani, C.; Betti, M. G. *J. Chem. Phys.* **2006**, *124*, 154702.
(30) Gargiani, P.; Angelucci, M.; Mariani, C.; Betti, M. G. *Phys. Rev. B* **2010**, *81*, 085412.
(31) Classen, T.; Fratesi, G.; Costantini, G.; Fabris, S.; Stadler, F. L.; Kim, C.; de Gironcoli, S.; Baroni, S.; Kern, K. *Angew. Chem.* **2005**, *117* (38), 6298−6301.
(32) Classen, T.; Lingenfelder, M.; Wang, Y.; Chopra, R.; Virojanadara, C.; Starke, U.; Costantini, G.; Fratesi, G.; Fabris, S.; de Gironcoli, S.; Baroni, S.; Haq, S.; Raval, R.; Kern, K. *J. Phys. Chem. A* **2007**, *111* (49), 12589−12603.
(33) Cossaro, A.; Cvetko, D.; Bavdek, G.; Floreano, L.; Gotter, R.; Morgante, A.; Evangelista, F.; Ruocco, A. *J. Phys. Chem. B* **2004**, *108* (38), 14671−14676.
(34) Perdew, J.; Burke, K.; Wang, Y. *Phys. Rev. B* **1996**, *54* (23), 16533−16539.
(35) Scandolo, S.; Giannozzi, P.; Cavazzoni, C.; de Gironcoli, S.; Pasquarello, A.; Baroni, S. *Z. Kristallogr.* **2005**, *220* (5−6), 574−579.
(36) Giannozzi, P.; Baroni, S.; Bonini, N.; Calandra, M.; Car, R.; Cavazzoni, C.; Ceresoli, D.; Chiarotti, G. L.; Cococcioni, M.; Dabo, I.; Dal Corso, A.; de Gironcoli, S.; Fabris, S.; Fratesi, G.; Gebauer, R.; Gerstmann, U.; Gougoussis, C.; Kokalj, A.; Lazzeri, M.; Martin-Samos, L.; Marzari, N.; Mauri, F.; Mazzarello, R.; Paolini, S.; Pasquarello, A.; Paulatto, L.; Sbraccia, C.; Scandolo, S.; Sclauzero, G.; Seitsonen, A. P.; Smogunov, A.; Umari, P.; Wentzcovitch, R. M. *J. Phys. Condens. Matter* **2009**, *21* (39), 395502.
(37) dos Reis, D.; Negreiros, F.; de Carvalho, V.; Soares, E. *Surf. Sci.* **2010**, *604* (5−6), 568−573.
(38) Tersoff, J.; Hamann, D. R. *Phys. Rev. Lett.* **1983**, *50*, 1998−2001.
(39) Koch, R.; Sturmat, M.; Schulz, J. *Surf. Sci.* **2000**, *454−456*, 543−551.
(40) Landmann, M.; Rauls, E.; Schmidt, W. G. *Phys. Rev. B* **2009**, *79* (4), 045412.
(41) Häberle, P.; Fenter, P.; Gustafsson, T. *Phys. Rev. B* **1989**, *39* (9), 5810−5818.

6257

dx.doi.org/10.1021/jp211036m | *J. Phys. Chem. C* 2012, 116, 6251−6258

(42) Ocko, B.; Helgesen, G.; Schardt, B.; Wang, J.; Hamelin, A. *Phys. Rev. Lett.* **1992**, *69* (23), 3350−3353.

(43) Michaelis, R.; Kolb, D. *Surf. Sci.* **1990**, *234* (3), L281−L284.

(44) Betti, M. G.; Gargiani, P.; Frisenda, R.; Biagi, R.; Cossaro, A.; Verdini, A.; Floreano, L.; Mariani, C. *J. Phys. Chem. C* **2010**, *114* (49), 21638−21644.

(45) Lu, X.; Hipps, K. W. *J. Phys. Chem. B* **1997**, *101* (27), 5391−5396.

(46) Sturmat, M.; Koch, R.; Rieder, K. *Phys. Rev. Lett.* **1996**, *77* (25), 5071−5074.

(47) Loffreda, D.; Sautet, P. *J. Phys. Chem. B* **2005**, *109* (19), 9596−9603.

(48) Nduwimana, A.; Gong, X.; Wang, X. *Appl. Surf. Sci.* **2003**, *219* (1−2), 129−135.

(49) Zhang, J.-M.; Li, H.-Y.; Xu, K.-W. *J. Phys. Chem. Solids* **2006**, *67* (8), 1623−1628.

(50) Yamaghishi, T.; Takahashi, K.; Onzawa, T. *Surf. Sci.* **2000**, *445* (1), 18−22.

(51) Cox, H.; Liu, X.; Murrell, J. *Mol. Phys.* **1998**, *93* (6), 921−924.

(52) Chui, Y. H.; Grochola, G.; Snook, I. K.; Russo, S. P. *Phys. Rev. B* **2007**, *75*, 033404.

(53) Todd, B.; Lyndenbell, R. *Surf. Sci.* **1993**, *281* (1−2), 191−206.

(54) Sun, J. T.; Gao, L.; He, X. B.; Cheng, Z. H.; Deng, Z. T.; Lin, X.; Hu, H.; Du, S. X.; Liu, F.; Gao, H.-J. *Phys. Rev. B* **2011**, *83*, 115419.

(55) Guaino, P.; Carty, D.; Hughes, G.; McDonald, O.; Cafolla, A. A. *Appl. Phys. Lett.* **2004**, *85* (14), 2777−2779.